Lytic Activity and Structural Differences of Amphipathic Peptides Derived from Trialysin[†,‡]

Rafael M. Martins,[§] Maurício L. Sforça,[∥] Rogério Amino,[⊥] Maria Aparecida Juliano,[+] Sérgio Oyama, Jr.,[∥] Luiz Juliano,[+] Thelma A. Pertinhez,[∥,@] Alberto Spisni,[*,∥,#] and Sergio Schenkman[*,§]

Departamento de Microbiologia, Imunologia e Parasitologia, Departamento de Bioquímica, and Departamento de Biofísica, Universidade Federal de São Paulo, R. Botucatu 862, São Paulo 04023-062, Brazil, Centro de Biologia Molecular Estrutural, Laboratório Nacional de Luz Síncrotron, Campinas, São Paulo 13083-100, Brazil, and Department of Experimental Medicine, University of Parma, Via Volturno, 39, Parma 43100, Italy

Received July 24, 2005; Revised Manuscript Received November 29, 2005

ABSTRACT: Trialysin is a pore-forming protein found in the saliva of *Triatoma infestans* (Hemiptera, Reduviidae), the insect vector of Chagas' disease. The protein is active against a broad range of cell types from bacteria to eukaryotic cells. Recognizing that the N-terminus of trialysin harbors the lytic motif [Amino, R., Martins, R. M., Procopio, J., Hirata, I. Y., Juliano, M. A., and Schenkman, S. (2002) *J. Biol. Chem. 277*, 6207−6213], we designed a set of peptides scanning this region to investigate the structural basis of its biological function. Peptides encompassing residues 1−32 (P6), 1−27 (P7), and 6−32 (P5) efficiently induced lysis of the protozoan parasite *Trypanosoma cruzi* and *Escherichia coli* in the 0.4−9.0 μM range, while much higher concentrations were required to cause hemolysis. Other more internal peptides, including peptide P2 (residues 21−47) and others up to residue 52, were less effective. P6 turned out to be the most active of all. P7 has a significantly higher activity than P5 against *E. coli*, while P5 has a hemolytic activity comparable to that of P6. CD spectroscopy showed that all tested peptides acquire a comparable helical content in solvent mixtures or in detergent micelles. The solution structure of P2 and P5−P7 was determined in a 30% trifluoroethanol/water mixture by nuclear magnetic resonance. All peptides exhibit a structure characterized by a central helical fold, and except for P2, which does not show a continuous hydrophobic surface, they are amphipathic. The structural models show that P5 and P7 extend their structural similarities with the most active peptide, P6, in either the C-terminus or the N-terminus. Amino acid substitutions in the N-terminus of P6 improved hemolysis but did not change the activity against *T. cruzi*. These results suggest that while amphipathicity is essential for the lytic activity, the selectivity of the active peptides for specific organisms appears to be associated with the structural features of their N- and C-termini.

To obtain its blood meal, *Triatoma infestans*, the insect vector of Chagas' disease, needs to overcome several barriers raised by the host. The first is physical, represented by the skin, and the second biochemical, represented by the hemostatic and inflammatory systems (*1*). For this reason, the salivary glands of these insects developed an ensemble of compounds aimed at this task, including, besides a sialidase (*2*), proteases (*3*), an anesthetic compound (*4*), anticoagulant proteins (*5*), and a pore-forming protein named trialysin (*6*). Since trialysin exerts its potent cytolytic activity on a large variety of cell types, from bacteria to mammalian cells, it has been hypothesized that it favors the maintenance of the salivary conduct free of microorganisms and parasites, among which is *Trypanosoma cruzi*, the agent of Chagas' disease.

The N-terminal region of trialysin has been predicted to form an amphipathic α-helix, and in a previous work (*6*), we have found that the peptide encompassing residues Gly6−Val32, P5 (Figure 1), possesses lytic activity, although it is ∼10 and ∼100 times less effective than the whole protein against trypanosomes and eukaryotic cells, respectively. The lytic domain of trialysin is reminiscent of the class of cationic lytic peptides found in the immune system and in the venoms of several animal species (*7*−*13*). Their mechanism of action is thought to occur either through pore formation, in which the peptides insert perpendicular to the plane of the membrane interacting with the lipid acyl chains, or through a carpet-like mode, in which they lie parallel to the membrane and act as a detergent (*14*). In either case, the peptides

[†] This work was supported by grants from Fundação de Amparo à Pesquisa do Estado de São Paulo (SMOLBnet) and Conselho Nacional de Desenvolvimento Científico e Tecnológico, Brazil.

[‡] The proton chemical shifts of P2 and P5−P7 have been deposited in the BMRB (http://www.bmrb.wisc.edu/) as entries 6859, 6616, 6618, and 6619, respectively.

* To whom correspondence should be addressed. S.S.: phone, (5511) 5575-1996; fax, (5511) 5571-5877; e-mail, sergio@ecb.epm.br. A.S.: phone, (39 0521) 033807; fax, (39 0521) 033802; e-mail, aspin@unipr.it.

[§] Departamento de Microbiologia, Imunologia e Parasitologia, Universidade Federal de São Paulo.

[∥] Laboratório Nacional de Luz Síncrotron.

[⊥] Departamento de Bioquímica, Universidade Federal de São Paulo.

[+] Departamento de Biofísica, Universidade Federal de São Paulo.

[@] Present address: Department of Experimental Medicine, Section of Chemistry and Structural Biochemistry, University of Parma, Parma, Italy.

[#] University of Parma.

10.1021/bi0514515 CCC: $33.50 © 2006 American Chemical Society
Published on Web 01/24/2006

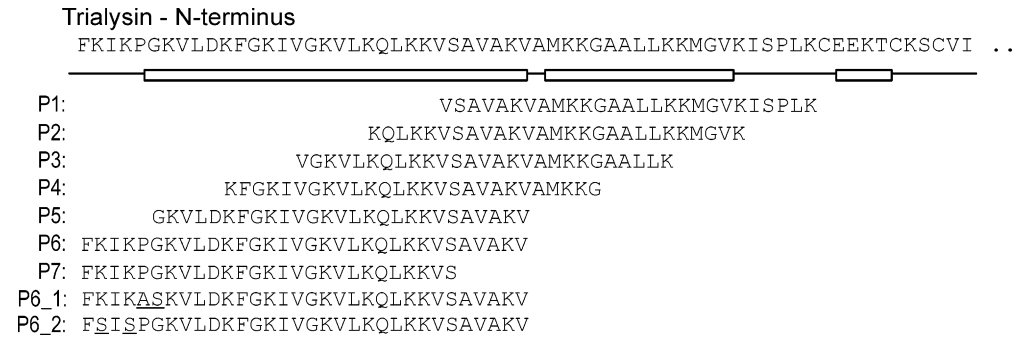

FIGURE 1: Synthetic peptides corresponding to the N-terminus of trialysin. The top sequence shows the N-terminal portion of mature trialysin. The boxes represent predicted amphiphilic α-helical regions (*53*). The sequences of peptides synthesized are aligned with respect to the protein sequence. Underlined residues correspond to mutated amino acids.

structural features and charge distribution as well as the composition of the target membrane are key determinants for lysis specificity (*15*, *16*).

Aiming to understand the lytic mechanism of trialysin, we have been prompted to search for its active motif. Here we present a study in which synthetic peptides encompassing portions of the N-terminus of trialysin have been tested for their lytic properties against the infective stage of *T. cruzi*, as well as against *Escherichia coli* and human erythrocytes. We found that the most active ones, independent of the target cell, are those encompassing the first 32 residues of the N-terminus of trialysin, in particular P6 (residues Phe1−Val32). As CD[1] spectroscopy indicated that all peptides acquire an α-helical fold both in the presence of detergent micelles and in TFE solutions, to highlight the possible existence of structural determinants that could justify their lytic specificity we selected the three most active ones together with one devoid of any activity and determined their structures in a 30/70 (v/v) TFE/water mixture by NMR spectroscopy.

EXPERIMENTAL PROCEDURES

Peptide Synthesis, Purification, and Quantitation. Peptides were synthesized by the Fmoc [*N*-(9-fluorenyl)methoxycarbonyl] methodology as previously described (*17*) using an automated benchtop simultaneous multiple solid-phase peptide synthesizer (PSSM 8 system from Shimadzu, Tokyo, Japan) and were purified to homogeneity by high-pressure liquid chromatography on a Vydac C18 analytical column. The molecular mass and sequence were checked by amino acid analysis, MALDI-TOF (TOFSpec E instrument from Micromass, Manchester, U.K.), and Edman degradation (PPSQ 23 system from Shimadzu). Peptide concentrations were determined from stock solutions by acid hydrolysis and amino acid analysis.

Trypanolytic Assay. Trypomastigote forms of *T. cruzi* (Y strain) were obtained from infected tissue cultures of LLC-MK_2 cells maintained at 37 °C in 5% CO_2 in Dulbecco's modified Eagle's medium supplemented with 10% fetal bovine serum. Serial dilutions of peptides were incubated with 3×10^6 culture trypomastigotes/mL at 37 °C for 1 h. The number of surviving (motile) parasites was determined in a Neubauer hemacytometer using a phase microscope (*6*).

Bactericidal Assay. E. coli DH5α was grown in Luria-Bertani liquid medium to an OD_{600} of 0.1 ($\sim 1.0 \times 10^8$ cells/mL) and incubated in the growth medium with each peptide at various concentrations for 1 h at 37 °C. The samples were then serially diluted in cold medium and plated. After overnight growth at 37 °C, colony-forming units were counted and plotted.

Hemolytic Assay. Erythrocytes were obtained from the cellular fraction of human blood collected with citrate and centrifuged at 2000*g* for 10 min, washed twice, and resuspended in Hanks solution containing 1% BSA. Serial dilutions of peptides were incubated with 3×10^7 erythrocytes/mL in U-bottomed 96-well plates at 37 °C for 2.5 h, under agitation. Plates were centrifuged at 2000*g* for 5 min, and the supernatants were collected. The amount of released hemoglobin was measured by reading the absorbance at 405 nm and compared to the total extent of lysis obtained with 0.2% Triton X-100.

CD Spectroscopy. Circular dichroism (CD) experiments were performed using a Jasco J-810 spectropolarimeter (JASCO International Co. Ltd., Tokyo, Japan), coupled to a Peltier Jasco PFD-425S system for temperature control. Samples were prepared by diluting a stock aliquot of the peptides to different concentrations in deionized water or TFE/H_2O mixtures or SDS micelles with the pH kept at 4.0. In the experiments carried out in the presence of SDS micelles, the SDS concentration was increased by addition of the required volume of a stock solution (400 mM SDS at pH 4.0). CD measurements were carried out using a 1 mm cell in the spectral range of 190−260 nm, at 37 °C. Each spectrum is the average of four consecutive scans. After baseline correction, concentration adjustment for dilution effects (in the case of SDS addition), and posterior confirmation of peptide concentration by amino acid analysis, the observed ellipticity, θ (millidegrees), was converted to the mean residue molar ellipticity, $[\theta]$ (degrees square centimeter per decimole). The percentage of α-helix was calculated as described previously (*18*).

NMR Spectroscopy. The samples for NMR measurements were prepared by dissolving P2 and P5−P7 in 600 μL of a TFE/H_2O (30/70, v/v) mixture, containing 5% D_2O, to yield a peptide concentration of approximately 1.2 mM at pH 4.0.

[1] Abbreviations: BMRB, BioMagResBank; CD, circular dichroism; cmc, critical micelle concentration; DQF-COSY, double-quantum-filtered correlation spectroscopy; LC_{50}, peptide concentration producing 50% lysis; LPC, palmitoyllysophosphatidylcholine; NMR, nuclear magnetic resonance; NOE, nuclear Overhauser effect; NOESY, nuclear Overhauser enhancement spectroscopy; rmsd, root-mean-square deviation; ROESY, rotating frame Overhauser spectroscopy; SDS, sodium dodecyl sulfate; TFE, trifluoroethanol; TOCSY, total correlation spectroscopy.

All two-dimensional ^{1}H NMR experiments were carried out in a Varian INOVA AS500 spectrometer operating at 499.730 MHz for the ^{1}H frequency at 37 °C. The proton chemical shifts were referenced to 4,4-dimethyl-4-silapentane-1-sulfonate (0.00 ppm). To assign the peptide resonance peaks, standard methods were used, including double-quantum-filtered correlation spectroscopy (DQF-COSY) (*19*), total correlation spectroscopy (TOCSY) (*20*), nuclear Overhauser enhancement spectroscopy (NOESY) (*21*, *22*), and rotating frame Overhauser spectroscopy (ROESY) (*23*) experiments. The TOCSY spectra were acquired using a DIPSI spin-lock sequence at a field strength of 10 kHz and a spin-lock evolution time of 75 ms. NOESY spectra with mixing times of 150, 200, 300, and 400 ms were recorded to evaluate the spin diffusion. ROESY experiments were recorded with mixing times of 100 and 150 ms.

All two-dimensional experiments were acquired in the phase-sensitive mode using the method of States (*24*). The spectral width was typically 6000 Hz, and 256 τ_1 increments, with 32 transients of 2048 complex points for each free induction decay, were recorded, except for the DQF-COSY experiment. It was collected with 1024 τ_1 experiments with 32 transients of 8192 complex points. Water suppression was achieved by low-power continuous wave irradiation during the relaxation delay. Solvent suppression in ROESY experiments was achieved using the WATERGATE method (*25*). Data were processed on a Silicon Graphics Octane 2 workstation using the nmrPIPE/nmrVIEW software (*26*). Prior to Fourier transformation, the time domain data were zero-filled in both dimensions to yield a 4K × 2K data matrix. When necessary, a fifth-order polynomial baseline correction was applied after transformation and phasing. To obtain distance constraints, cross-peak volumes were estimated from the 300 ms (P2 and P6) or 400 ms (P5 and P7) NOESY spectra and 100 ms (P6) or 150 ms (P2, P5, and P7) ROESY spectra. To relate them to interproton distances, a calibration was made using the distance of 1.8 Å for the well-defined geminal β-protons, and the NOE volumes were classified as strong, medium, and weak, corresponding to the upper bound constraints of 2.8, 3.5, and 5.0 Å, respectively. Lower bounds were taken to be the sum of the van der Waals radii (1.8 Å) for the interacting protons in all cases.

Molecular Modeling. The three-dimensional structures of all peptides were computed using the simulated annealing methods in the DYANA refine module (*27*). The modeling protocol was based on the method implemented by Pristovšek et al. (*28*). Each round of refinement started with 20 random conformers, from which the 10 lowest-target function structures were used to analyze constraint violations and assign additional NOE constraints to be included in the subsequent calculation. This process was repeated until all violations were eliminated. In the final round of refinement, a total of 200 structures were calculated and the 40 conformers with the lowest target function were considered for analysis. After simulated annealing, these 40 structures with a target function smaller than 0.11 ± 0.010 (P2), 0.28 ± 0.016 (P5), 0.20 ± 0.020 (P6), and 0.17 ± 0.016 Å^2 (P7), with no distance violation larger than 0.2 Å and no dihedral angle violation greater than 5°, were energy minimized with a full consistent valence force field (*29*, *30*) (Morse and Lennard-Jones potentials, Coulombic term) using, in the early stages of refinement, 1500 steps per structure and steepest descents until the maximum derivative was less than 1000 kcal/Å. In the final round, 15 000 steps were carried out using conjugated gradients until the maximum derivative was less than 0.001 kcal/Å. All calculations were carried out on a Silicon Graphics Octane 2 workstation using the DISCOVER software package, together with INSIGHT II as the graphic interface (Accelrys Inc., San Diego, CA). The quality of the final structures was analyzed using PROCHECK-NMR (*31*) and CNS (*32*).

Table 1: Physical Properties of Trialysin-Derived C-Terminally Amidated Peptides

peptide	molecular mass[a] (Da)	charge[a] pH 7.0	charge[a] pH 4.0	mean hydrophobicity[b] CSS[c]	Kyte−Doolittle[d]	Eisenberg[e]
P1	2782.5	+5.9	+6.1	−0.95	−0.23	−0.24
P2	2869.6	+7.9	+8.1	−2.07	−0.71	−0.41
P3	2822.6	+6.9	+7.1	−1.35	−0.45	−0.32
P4	2899.6	+7.9	+8.1	−1.76	−0.78	−0.39
P5	2896.6	+5.9	+6.3	−1.31	−0.72	−0.33
P6	3510.4	+7.9	+8.3	−1.15	−0.76	−0.35
P7	3041.8	+6.9	+7.3	−1.22	−0.9	−0.4
P6_1	3517.4	+8.9	+9.5	−1.24	−0.61	−0.35
P6_2	3431.2	+6.9	+7.5	−0.8	−0.53	−0.25

[a] Predictions made by Protean from the DNAstar package. [b] Calculated using the analysis tool of Tossi and Sandri (see http://www.bbcm.units.it/~tossi/HydroCalc/HydroMCalc.html). [c] As defined in ref *51*. [d] As defined in ref *52*. [e] As defined in ref *53*.

RESULTS

Peptide Design. Secondary structure prediction indicates that the N-terminal portion of the mature trialysin should form two amphiphilic α-helices extending from Gly6 to Val32 and from Met34 to Val46 (Figure 1). As peptide P5 was shown to induce lysis of *T. cruzi* and erythrocytes (*6*), to search for the minimal lytic motif in this region, we selected and synthesized the peptides, in their amidated form, as shown in Figure 1. Table 1 reports the chemical and physical properties of the peptides.

Biological Activities. The peptide's lytic activity has been tested after incubation for 1 h at 37 °C against the trypomastigote form of *T. cruzi* (Figure 2A) and *E. coli* (Figure 2B) and after incubation for 2.5 h with human erythrocytes (Figure 2C). Parasite lysis was observed at 0.2 μM P6, with 100% lysis at 2 μM. Bacterial lysis started at 2 μM, reaching total lysis at ∼10 μM, while higher concentrations of P6 (from 50 to 200 μM) were required to lyse erythrocytes. Other peptides were less efficient. To compare the lytic activity of the various peptides, we estimated their LC_{50} values (Table 2) and considered the value obtained for the most active peptide (P6) to be 100%. As reported in Figure 2D−F, the peptides encompassing the trialysin region, residues Phe1−Val32 (P5−P7; see Figure 1), are the most active ones. Interestingly, however, while P6 is the most effective of all against *T. cruzi*, in the case of *E. coli*, we found that P7 exhibits an activity that is only 50% lower and that P5 is as lytic as P6 against erythrocytes. Peptides P1−P3 encompassing regions of trialysin farther from the N-terminus, between residues Val16 and Lys52 (Figure 1), exhibit much lower activity against *T. cruzi*, and they are practically inactive against bacteria and erythrocytes. P4, residues Lys11−Gly37, has an intermediate activity toward all targets.

To quantify the specificity of an antimicrobial agent, it is common to use the therapeutic index. This parameter is the

Table 2: Lytic Activities of the Synthetic Peptides

peptide	LC_{50} [μM (μg/mL)][a]			safety index[b]	
	T. cruzi	*E. coli*	erythrocytes	erythrocytes/ *T. cruzi*	erythrocytes/ *E. coli*
P1	15 (41.7)	33 (91.8)	>900 (>2500)	–	–
P2	6 (17.2)	>50 (>143)	450 (1290)	75	–
P3	19 (53.6)	>50 (>141)	>900 (>2500)	–	–
P4	6 (17.3)	7.6 (22.0)	274 (794)	46	36
P5	1.6 (4.6)	9 (26.1)	117 (338)	73	13
P6	0.4 (1.4)	2.6 (9.1)	90 (316)	225	35
P7	1.3 (4.0)	5.2 (15.8)	296 (900)	227	57
P6_1	0.4 (1.4)	0.9 (3.2)	12.6 (44.3)	31.5	14.7
P6_2	0.9 (3.1)	1.7 (5.8)	28.1 (96.4)	31.2	16.3

[a] The LC_{50} was taken from the curves of Figure 2 as the peptide concentration required to lyse 50% of the target cells. [b] Safety indexes were calculated using the LC_{50} (micromolar) reported in this table when precisely determined.

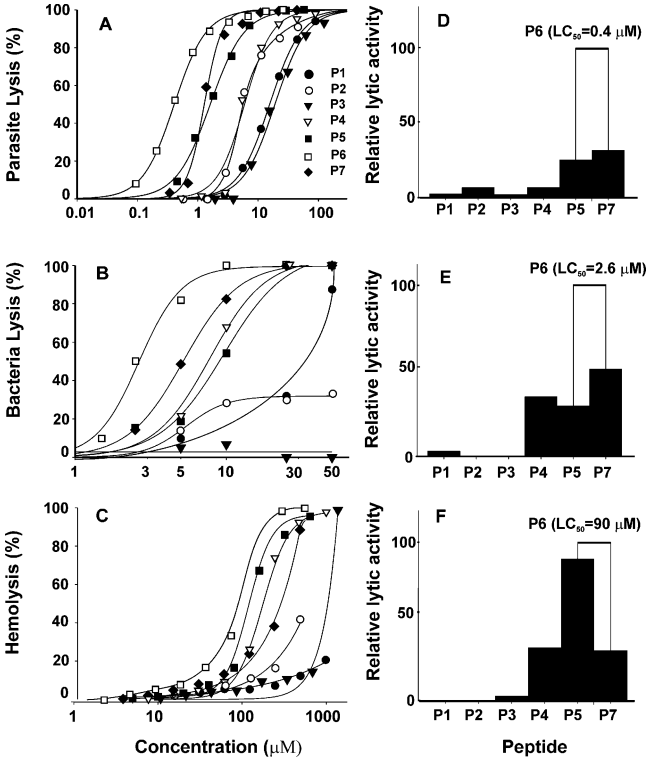

FIGURE 2: Peptide lytic activity. Peptides were incubated at 37 °C with trypomastigote forms of *T. cruzi* (A), *E. coli* (B), and human erythrocytes (C), at the indicated concentrations. Lysis was assessed after 1 h for *T. cruzi* and *E. coli* or 2.5 h for erythrocytes as described in Experimental Procedures. The LC_{50} values obtained from the lysis curves were used to compare peptide activities for *T. cruzi* (D), *E. coli* (E), and erythrocytes (F). The LC_{50} of the most active peptide (P6) is indicated as a white bar, and it has been taken to be 100%. The LC_{50} values of the others peptides (black bars) have been plotted accordingly.

ratio of the minimal hemolytic concentration (MHC) and the minimal inhibitory concentration (MIC), the concentration that totally inhibits bacterial growth (*33*). Here, the analysis of the concentration dependence of the lytic activity reported in Figure 2 suggests that another possible way to effectively highlight the antimicrobial efficiency and the associated reduced hemolytic damage is the ratio between the LC_{50} for erythrocytes and the one for bacteria or parasites, which we call the "safety index". The larger the value, the better it is from a therapeutical point of view. Table 2 reports these values for the studied peptides. As can be seen, peptides P6 and P7 appear to be the ones with the best features, having a very low LC_{50} and a high safety index.

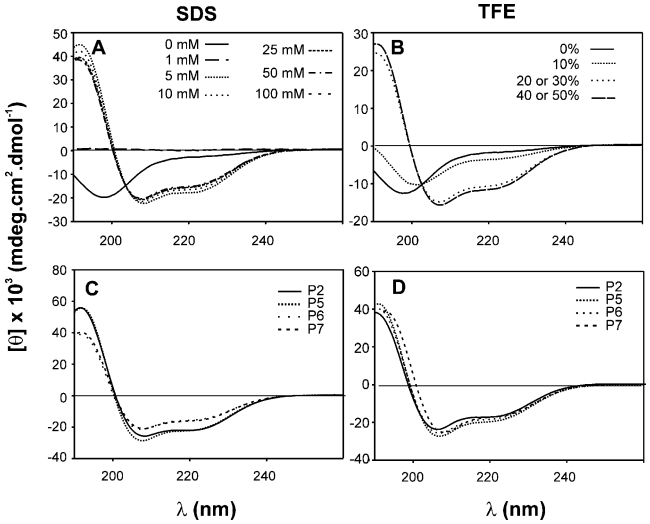

FIGURE 3: Peptide CD spectra. P6 was diluted to 70 μM in the indicated concentrations of SDS (A) or TFE (B). Panels C and D show the spectra of 70 μM P2 and P5−P7 in 100 mM SDS and 30% TFE. All experiments were carried out at 37 °C and pH 4.0, unless otherwise stated.

CD Analysis. All peptides in water exhibit a random coil conformation, and no peptide or salt concentration dependence has been detected (data not shown). However, in the presence of both SDS at concentrations above 5 mM (SDS cmc ~ 3−4 mM) and a TFE/water mixture above 20% TFE (v/v), we found that they all fold into an α-helical conformation as indicated by the two negative bands at 208 and 222 nm and by the positive one at 194 nm. Panels A and B of Figure 3 report, as an example, the titration of P6 with SDS and TFE, respectively. Panels C and D of Figure 3 report the CD spectra of P2 and P5−P7 in 100 mM SDS and in a 30% (v/v) TFE/water mixture, respectively. A similar CD pattern was observed also for P1, P3, and P4 (data not shown). CD spectra of P2 and P5−P7 indicate that, also in the presence of LPC micelles, the peptides acquire an α-helical fold (data not shown).

NMR Spectroscopy. The initial attempts to determine the solution structure of P6 in SDS or LPC micelles were not successful. In fact, the resonance lines of the amide protons in the monodimensional ^{1}H NMR experiments turned out to be broad under all the experimental conditions that were tested (data not shown), thus suggesting that the peptide, at the concentration used for the NMR experiments, has a propensity to aggregate. The similarity of the peptides CD

spectra in TFE and in the presence of detergent micelles (Figure 3) suggest they acquire a comparable helical conformation, and because at this stage our goal was to determine the solution structure of the peptides in their monomeric state, the NMR experiments have been carried out in a TFE/H_2O mixture (30/70, v/v). Peptides P5−P7 were selected as they are the most active and because their lytic activity evidenced a diverse selectivity for each of the chosen targets. We also determined the solution structure of P2 because it is practically devoid of activity against all targets.

The ^{1}H resonance sequential assignment was achieved on the basis of TOCSY, COSY, NOESY, and ROESY two-dimensional spectra, and the chemical shifts for each peptide have been deposited in the BMRB as accession numbers 6859, 6616, 6618, and 6619 for P2 and P5−P7, respectively.

Secondary Structure. The summary of the inter-residue NOEs is reported in Figure 4. Peptides P5−P7 present strong $d_{NN}(i,i+1)$ NOEs together with a dense pattern of $d_{\alpha N}(i,i+3)$, $d_{\alpha\beta}(i,i+3)$, and $d_{\alpha N}(i,i+4)$ NOEs involving residues Lys11−Leu23, indicating they all possess an α-helical fold in that region. However, while for P6 the α-helix extends back to Gly6 and up to Ser27, for P5 the helix extends only from Lys24 to Val29. In the case of P7, in addition to the central α-helical region common to the other two peptides, there is instead a slight indication of helical secondary structure involving residues Val8−Asp10. For P2, the intense $d_{NN}(i,i+1)$ and the very dense $d_{\alpha N}(i,i+3)$, $d_{\alpha\beta}(i,i+3)$, and $d_{\alpha N}(i,i+4)$ pattern indicate the presence of an α-helix encompassing most of the peptide, residues Lys25−Met44. For all peptides, the weaker $d_{\alpha N}(i,i+1)$, as compared to $d_{NN}(i,i+1)$ connectivities, and a well-defined pattern of medium-range NOEs indicate that their central helical fold is quite stable.

Molecular Modeling. A total of 321, 384, 305, and 398 distance restraints, including 73, 74, 59, and 126 medium-range, for P5−P7 and P2, respectively, were used for structure calculations using DYANA (*27*). After energy minimization, 15 models for P5−P7 and 18 models for P2 were chosen on the basis of the lowest rmsd and used to represent the solution three-dimensional structure of each peptide. Table 3 summarizes the structural statistics of these four peptides. The Ramachandran plot analysis shows that all the φ and ψ angles are in allowed regions. In addition, there are no significant violations of molecular geometry parameters. Figure 5A shows the superimposition of the selected models for the three peptides in the Lys11−Leu23 region where they all exhibit an α-helical fold as already suggested by the NOE pattern (Figure 4). The rmsd's for the backbone and for the heavy atoms are quite low (Table 3), confirming the good definition of the helix. As indicated by the NOE pattern (Figure 4), the α-helical region extends differently in P5 with respect to P6 and P7. The rmsd's obtained for the superposition of residues Lys11−Val29 for P5 and Val8−Leu23 for P6 and P7 are still quite satisfactory, indicating that the helical fold is well-defined also in these extended regions (Table 3). A visual inspection of Figure 5A, however, evidences that the three peptides differ in the degree of conformational flexibility of their N- and C-termini, with P5 exhibiting a reduced spread. Figure 5B shows that peptide P2 exhibits a regular and well-defined α-helical structure involving most of the peptide sequence, Lys25−Gly45, as indicated by the low rmsd (Table 3).

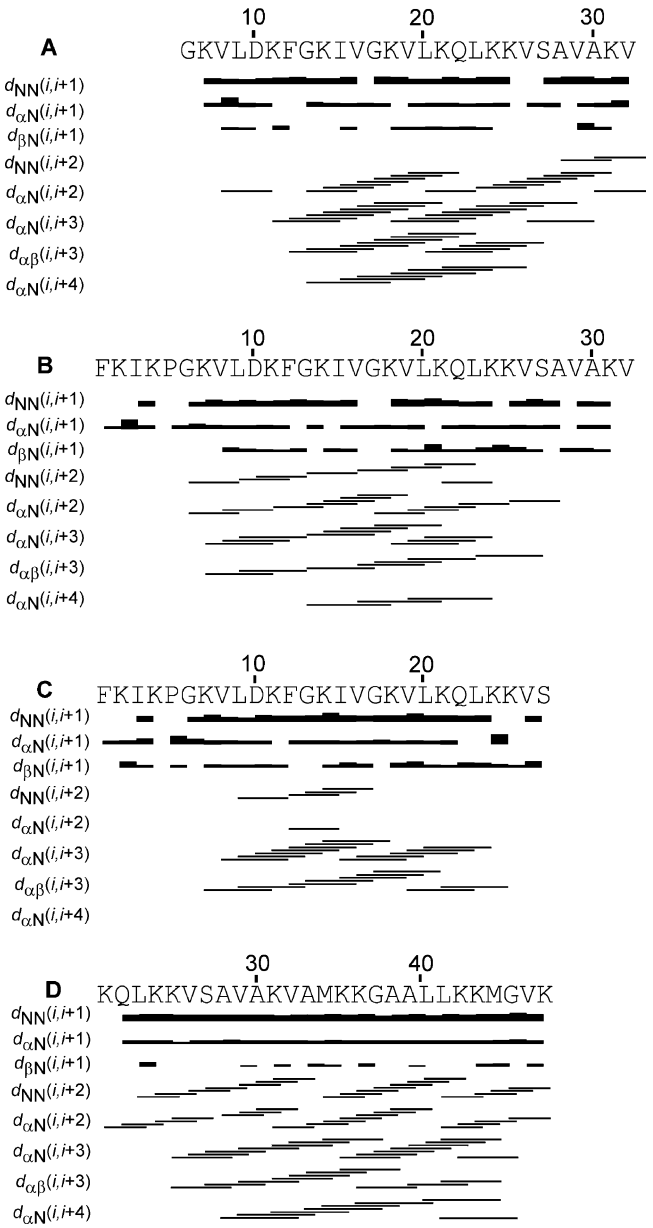

FIGURE 4: Summary of the sequential and medium-range NOE connectivities for P5 (A), P6 (B), P7 (C), and P2 (D) in a TFE/H_2O (30/70, v/v) mixture at 37 °C and pH 4.0. Only the sequences of peptides P5−P7 are aligned. The intensities of the observed NOEs are represented by the thicknesses of lines and are classified as strong, medium, and weak, corresponding to upper bound constraints of 2.8, 3.5, and 4 Å, respectively.

Recognizing that P5−P7 present a structurally similar central region and that, perhaps, the origin of their differentiated lytic activity is associated with their N- or C-termini, we selected the minimum energy model of each peptide and superimposed their backbones. Figure 6A reports the results of this comparison. As seen here, besides the central region, P6 and P5 show a good superimposition in the Lys24−Ala30 region, with a rmsd for the backbone as low as 0.37 Å (Table 3). On the other hand, P6 and P7 exhibit a quite satisfactory superposition in the Ile3−Asp10 region, where the rmsd = 1.14 Å (Table 3). Overall, a good superposition is found in the Lys11−Ala30 and Lys2−Leu23 regions for P6 and P5, and P6 and P7, respectively (Table 3). Interestingly, a good match is found also for the side chains of the N- and C-terminal regions (Figure 6B,C).

Table 3: Structural Statistics of the NMR-Derived Structures of P2 and P5−P7

	P2	P5	P6	P7
no. of structures	18	15	15	15
no. of NOE-based distance constraints				
total distance	398	321	384	305
intraresidue	190	172	235	132
sequential	82	76	75	114
medium-range	126	73	74	59
rmsd from ideal covalent geometry				
bonds (Å)	−	0.0046	0.0036	0.0036
angles (deg)	−	0.5661	0.5123	0.4815
impropers (deg)	−	0.3147	0.1953	0.2411
dihedrals (deg)	−	26.6225	27.7814	27.7273
Ramachandran plot analysis				
most favored region (%)	86.5	87.5	82.7	85.1
additionally allowed region (%)	13.5	12.5	17.3	14.9
generously allowed region (%)	0	0	0	0
disallowed region (%)	0	0	0	0
rmsd (Å)				
backbone (residues)[a]	1.17 ± 0.31 (all)	0.43 ± 0.07 (11−29)	0.44 ± 0.20 (8−23)	0.20 ± 0.07 (8−23)
	0.40 ± 0.11 (25−45)	0.28 ± 0.06 (11−23)	0.28 ± 0.10 (11−23)	0.14 ± 0.04 (11−23)
heavy atoms (residues)[a]	2.16 ± 0.53 (all)	1.17 ± 0.15 (11−29)	1.18 ± 0.38 (8−23)	1.12 ± 0.20 (8−23)
	1.17 ± 0.18 (25−45)	0.96 ± 0.13 (11−23)	1.16 ± 0.37 (11−23)	1.18 ± 0.22 (11−23)

	rmsd (Å) (minimum energy)	
	P5 and P6	P6 and P7
backbone (residues)	1.00 (11−30)	1.67 (2−23)
	0.37 (24−30)	1.14 (2−10)
heavy atoms (residues)	2.47 (11−30)	3.47 (2−23)
	1.78 (24−30)	2.08 (2−10)

[a] Values in parentheses correspond to the residues used for superimposition.

DISCUSSION

In a previous work, we showed that the N-terminus of trialysin contains regions that must be involved with the protein antimicrobial/lytic activity (*6*). The data presented here evidence that, of the seven peptides that were tested, encompassing selected regions of the first 52 N-terminal residues, three of them, P5−P7, that map the trialysin Phe1−Val32 region exhibit remarkable lytic activity against *T. cruzi* trypomastigotes, *E. coli*, and, to a lesser extent, erythrocytes. P4, corresponding to residues Lys11−Gly37, turns out to be poorly active against the parasite *T. cruzi*, although its lytic activity is comparable to that of P5 and P7 against bacteria and erythrocytes, respectively. P1−P3, covering the trialysin Val16−Lys52 region, are much less active against all targets.

These peptides have a comparable mass, and their total charges range between 5.9 and 7.9 at physiological pH. Moreover, their mean hydrophobicities, calculated using the various methods available at http//www.bbcm.it/∼tossi/HydroCalc/HydroMCalc.html, do not evidence any significant difference that can be correlated to their diverse biological activity (Tables 1 and 2). Since the CD data indicate that they are all capable of acquiring a comparable helical fold both in TFE and in the presence of detergent micelles (Figure 3), we can infer that the peptide functional differences may be related to other conformational features.

Peptide antimicrobial activity is generally associated with their ability to acquire an amphipathic α-helical conformation and to possess a positively charged surface. Indeed, as shown in Figure 7A, the hydrophobic/hydrophilic surfaces obtained using Insight II confirm that peptides P5−P7 acquire amphipathic structures. Interestingly, unlike P5, the nonlytic peptide P2 does not present a clear amphipathic nature (Figure 8), which explains its poor lytic activity. Overall, these results confirm that the presence of an amphipathic helix is a requirement for expressing significant lytic activity (*34*). Despite its lytic activity against *E. coli* and erythrocytes, peptide P4, which has part of the amphipathic helix of P5, was not investigated because it is practically devoid of any lytic effect against trypanosomes.

By comparing the lytic efficiency of P5−P7, peptide P6 is the most potent of all with an LC_{50} ranging from 0.4 μM against *T. cruzi* up to 90 μM against erythrocytes, a trend common to the three peptides. Interestingly, however, while P5 and P7 are much less effective than P6 against *T. cruzi*, P7 exhibits a significant activity against *E. coli*, being only half that observed for P6, and P5 is as active as P6 against erythrocytes. From a structural point of view, though they all share the same well-defined helical fold in their central part (Figure 5), it is worth noticing that the NMR data reveal that P6 and P5 exhibit the same structure in the C-terminus while P6 and P7 possess the same conformational organization in the N-terminus (Figure 6). In other words, P6 and P5 present a similar conformation in their central and C-terminal regions (rmsd for backbone residues Lys11−Ala30 = 1.00 Å), while P6 and P7 exhibit a superimposable backbone in their N-terminal and central regions (rmsd for backbone residues Lys2−Leu23 = 1.67 Å). These structural similarities at the N- and C-termini also involve the amino acid side chains (Figure 6B,C).

Recently, it has been proposed that the increasing peptide positive charge and amphipathicity are important for bacterial lysis while an increase in hydrophobicity correlates with erythrocyte lysis (*33*). Indeed, our results corroborate these reports as the analysis of the electrostatic surface of P5−P7 using MOLMOL (*35*) evidences they have large positively

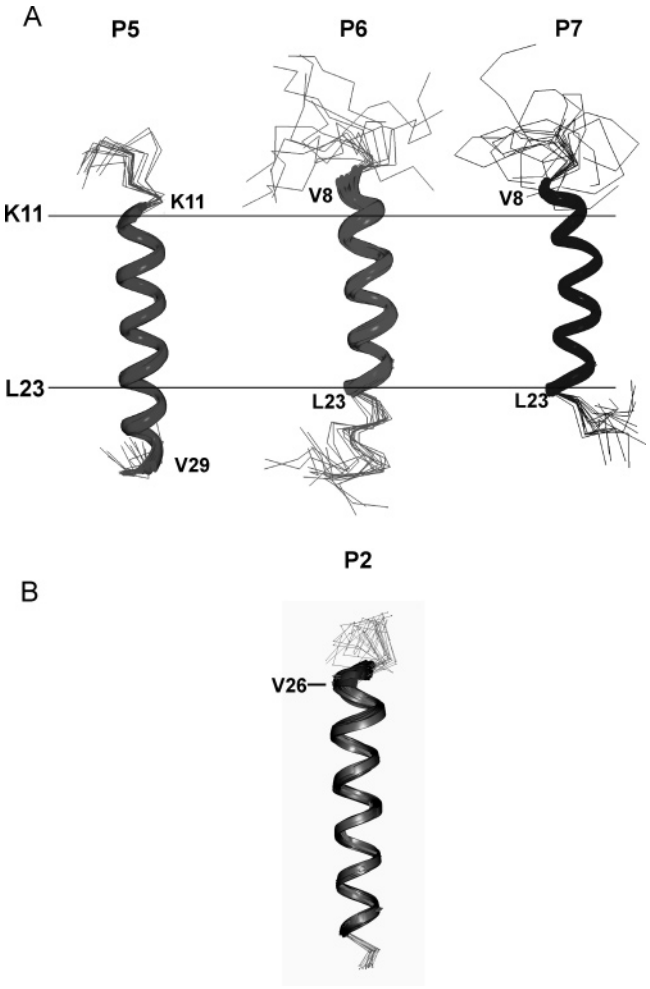

FIGURE 5: Peptide solution structure. (A) Backbone superposition of the final 15 minimum-energy models of P5−P7 in a TFE/H_2O (30/70, v/v) mixture at 37 °C and pH 4.0. The horizontal lines indicate the position of residues Lys11 and Leu23 of peptides. (B) Backbone superposition of the final 18 minimum-energy models of P2 in a TFE/H_2O (30/70, v/v) mixture at 37 °C and pH 4.0.

charged patches (Figure 7B), and in fact, they are more active against bacteria and parasites than against erythrocytes. In addition, inconsistent with the hypothesis of the existence of a direct correlation between peptide helicity and hemolytic activity (*14*), here we find that, despite the comparable helicity (Figure 5) and hydrophobicity (Table 1), P5−P7 exhibit diverse hemolytic activities as well as a diverse selectivity for bacteria and parasites, thus suggesting other factors must be considered. P2, on the other hand, is not amphipathic (Figure 8A). It is mainly neutral (Figure 8B) and, as a result, is devoid of any significant lytic activity against all targets.

Thus, we propose that the diversified lytic activity against the selected targets may be associated with the presence of specific structural details. The relatively higher antimicrobial/antiparasitic effectiveness (as revealed by the combined evaluation of the LC_{50} and of the safety index) of P6 and P7, compared to that of P5, might be due to the presence of an N-terminal segment that folds into some nonconventional structural elements (bends or hydrophobic clusters), as it has been found for an antimicrobial peptide derived from bovine hemoglobin (*36*). In P5, the absence of this type of N-terminus and the concomitant presence of a more extended well-defined α-helical arrangement in the C-terminus, present

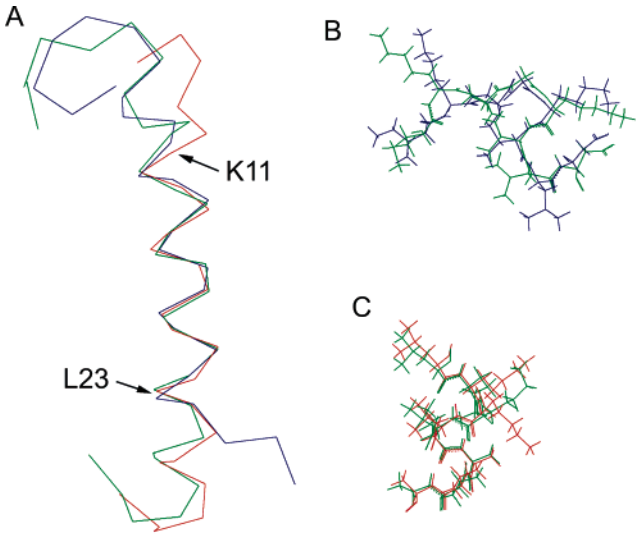

FIGURE 6: (A) Selective backbone superposition of P5−P7. (B) Superposition of the backbone and side chains, residues 3−10, of peptides P6 and P7. (C) Superposition of the backbone and side chains, residues 24−30, of peptides P5 and P6. The color coding is as follows: P6 colored green, P7 blue, and P5 red.

also in P6, could justify their similar high lytic activity against erythrocytes. The fact that P6 contains all these structural features would explain its overall higher lytic efficiency against all targets. Moreover, results showing that modifications introduced into the N-terminus of P6 reduced the safety index further support the notion of the role played by this peptide region. Interestingly, replacement of Pro5 and Gly6 with Ala and Ser, respectively, enhances the peptide's hemolytic activity, without affecting its trypanolysis efficiency (Table 2). Though proline is known to have a role in antimicrobial peptides when located in the middle of the peptide (*37*, *38*), the effect observed in this case cannot be explained simply on the basis of a reduced backbone flexibility. In fact, substitution of Lys2 and Lys4 with Ser produces a comparable effect (Table 2).

Recognizing that the cell membrane is the main target of antimicrobial peptides, we may hypothesize that the diverse lipid composition and distribution or the presence of others components in the cell membrane of the various organisms play an important role in the modulation of peptide−membrane interaction, thus leading to the differentiation of their action. Indeed, while *T. cruzi* membrane composition is characterized mainly by zwitterionic/neutral lipids (*39*), the erythrocyte cell membrane contains a considerable amount of cholesterol, which confers rigidity to the membrane, and small amounts of negative lipids. In contrast, the *E. coli* plasma membrane contains a significant amount of negatively charged phospholipids, particularly 20% phosphatidylglycerol (*40*). More than that, while the surface of *T. cruzi* is covered by sialylated mucin-like glycoproteins (*41*), bacteria present lipopolysaccharides and erythrocytes glycoproteins. Indeed, it is well-known that peptides such as melittin, which has affinity for both anionic and zwitterionic lipids, exhibit a broad range of activity, from bacteria to erythrocytes (*11*), while magainin, which interacts selectively with the anionic lipids on the outer leaflet of the plasma membrane, is highly effective against microorganisms and a poor hemolytic agent (*42*). Thus, if we combine these observations with the fact that C-terminally amidated pep-

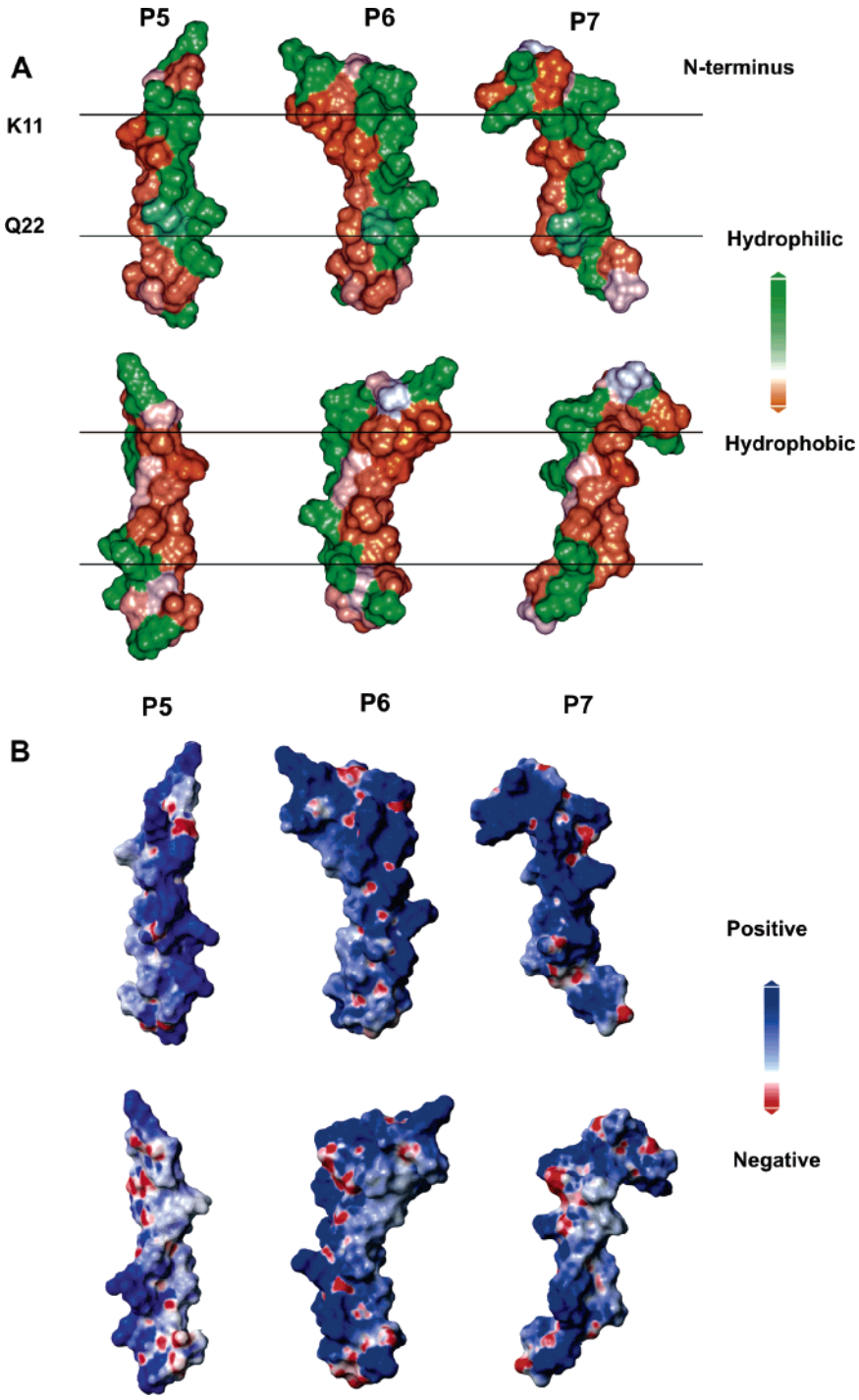

FIGURE 7: (A) Hydrophobic/hydrophilic surface obtained using Insight II (*30*) for the minimum-energy structure of P5−P7 in a TFE/H_2O (30/70, v/v) mixture at 37 °C and pH 4.0. (B) The electrostatic surface of the peptides was obtained using MOLMOL (*35*). The bottom structures represent the peptides rotated 180° around their longitudinal axis.

tides exhibit an enhanced antimicrobial activity due to a reduced structural flexibility of the peptide C-terminal region (ref *12* and a manuscript in preparation), it is conceivable to envisage that the existence of a synergistic effect between the presence of structural details involving the peptide termini and the diverse lipid composition of the membrane that characterize the various antimicrobial peptide target organisms will lead to a differentiation of their selectivity and efficiency.

Overall, in view of the increasing bacterial resistance to conventional antibiotics, antimicrobial peptides have been identified as a promising alternative (*43*) as they act on a target against which it is difficult to generate resistance, the plasma membrane. So far, they have been tested against a wide range of microorganisms, even cancer cells, but protozoa have often been overlooked with the exception of some applications in parasitic infections such as *Leishmania* spp. and the malaria-causing parasites, *Plasmodium* spp. (*44*). Melittin (*45*), magainins (*46*), cecropins (*47*), dermaseptins (*48*), phylloseptins (*49*), and even a peptide from NK-lysin, a T lymphocyte protein (*50*), are active against *T. cruzi* at concentrations ranging from 2.5 μM (NK-2 peptide) to 20 mM (magainins). Since the goal is to devise molecules active against parasites and bacteria at very low concentrations that

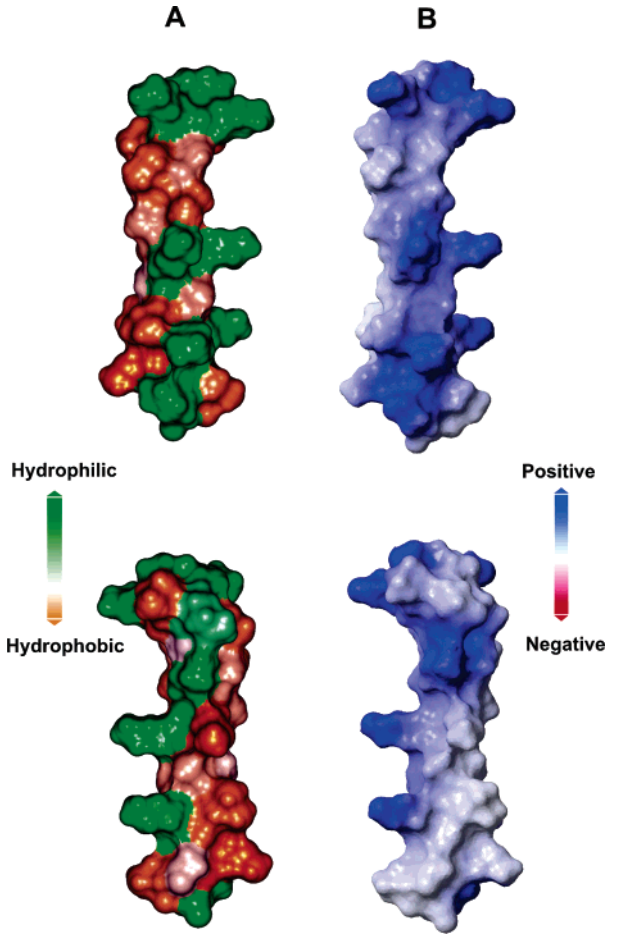

FIGURE 8: Minimum-energy NMR-derived solution structure of peptide P2. (A) The hydrophobic/hydrophilic surface was obtained using Insight II (*30*). (B) The electrostatic surface was obtained using MOLMOL (*35*). The bottom structures represent the peptides rotated 180° around their longitudinal axis.

are harmless to mammalian host cells, on the basis of this work, it appears that P7 and P6, due to their very low LC_{50} against parasites and bacteria as well as their high safety index (Table 2), are promising peptides for biomedical application.

ACKNOWLEDGMENT

We thank Evania Barbosa Azevedo for technical support, Izaura Yoshico Hirata (Departamento de Biofísica, UNIFESP) for the peptide amino acid analysis, and Bruno dos Santos Pascoalino and Gabriel Andrade Alves for help with the bacterial lysis assays.

REFERENCES

1. Ribeiro, J. M. (1995) Blood-feeding arthropods: Live syringes or invertebrate pharmacologists? *Infect. Agents Dis. 4*, 143−152.
2. Amino, R., Porto, R. M., Chammas, R., Egami, M. I., and Schenkman, S. (1998) Identification and characterization of a sialidase released by the salivary gland of the hematophagous insect *Triatoma infestans*, *J. Biol. Chem. 273*, 24575−24582.
3. Amino, R., Tanaka, A. S., and Schenkman, S. (2001) Triapsin, an unusual activatable serine protease from the saliva of the hematophagous vector of Chagas' disease *Triatoma infestans* (Hemiptera: Reduviidae), *Insect Biochem. Mol. Biol. 31*, 465−472.
4. Dan, A., Pereira, M. H., Pesquero, J. L., Diotaiuti, L., and Beirao, P. S. (1999) Action of the saliva of *Triatoma infestans* (Heteroptera: Reduviidae) on sodium channels, *J. Med. Entomol. 36*, 875−879.
5. Pereira, M. H., Souza, M. E., Vargas, A. P., Martins, M. S., Penido, C. M., and Diotaiuti, L. (1996) Anticoagulant activity of *Triatoma infestans* and *Panstrongylus megistus* saliva (Hemiptera/Triatominae), *Acta Trop. 61*, 255−261.
6. Amino, R., Martins, R. M., Procopio, J., Hirata, I. Y., Juliano, M. A., and Schenkman, S. (2002) Trialysin, a novel pore-forming protein from saliva of hematophagous insects activated by limited proteolysis, *J. Biol. Chem. 277*, 6207−6213.
7. Lehrer, R. I., and Ganz, T. (1999) Antimicrobial peptides in mammalian and insect host defence, *Curr. Opin. Immunol. 11*, 23−27.
8. Bulet, P., Töcklin, R., and Menin, L. (2004) Anti-microbial peptides: From invertebrates to vertebrates, *Immunol. Rev. 198*, 169−184.
9. Kuhn-Nentwig, L. (2003) Antimicrobial and cytolytic peptides of venomous arthropods, *Cell. Mol. Life Sci. 60*, 2651−2668.
10. Hultmark, D., Steiner, H., Rasmuson, T., and Boman, H. G. (1980) Insect immunity. Purification and properties of three inducible bactericidal proteins from hemolymph of immunized pupae of *Hyalophora cecropia*, *Eur. J. Biochem. 106*, 7−16.
11. Dempsey, C. E. (1990) The actions of melittin on membranes, *Biochim. Biophys. Acta 1031*, 143−161.
12. Sforça, M. L., Oyama, S., Jr., Canduri, F., Lorenzi, C. C., Pertinhez, T. A., Konno, K., Souza, B. M., Palma, M. S., Ruggiero, N. J., Azevedo, W. F., Jr., and Spisni, A. (2004) How C-terminal carboxyamidation alters the biological activity of peptides from the venom of the eumenine solitary wasp, *Biochemistry 43*, 5608−5617.
13. Zasloff, M. (1987) Magainins, a class of antimicrobial peptides from *Xenopus* skin: Isolation, characterization of two active forms, and partial cDNA sequence of a precursor, *Proc. Natl. Acad. Sci. U.S.A. 84*, 5449−5453.
14. Shai, Y. (1999) Mechanism of the binding, insertion and destabilization of phospholipid bilayer membranes by α-helical antimicrobial and cell non-selective membrane-lytic peptides, *Biochim. Biophys. Acta 1462*, 55−70.
15. Dathe, M., and Wieprecht, T. (1999) Structural features of helical antimicrobial peptides: Their potential to modulate activity on model membranes and biological cells, *Biochim. Biophys. Acta 1462*, 71−87.
16. Sitaram, N., and Nagaraj, R. (1999) Interaction of antimicrobial peptides with biological and model membranes: Structural and charge requirements for activity, *Biochim. Biophys. Acta 1462*, 29−54.
17. Hirata, I. Y., Cezari, M. H. S., Nakaie, C. R., Boschov, P., Ito, A. S., Juliano, M. A., and Juliano, L. (1994) Internally quenched fluorogenic protease substrates: Solid-phase synthesis and fluorescence spectroscopy of peptides containing *ortho*-aminobenzoyl/dinitrophenyl groups as donor−acceptor pairs, *Lett. Pept. Sci. 1*, 299−308.
18. Chen, Y. H., Yang, J. T., and Chau, K. H. (1974) Determination of the helix and β form of proteins in aqueous solution by circular dichroism, *Biochemistry 13*, 3350−3359.
19. Piantini, U., Sorensen, O. W., and Ernst, R. R. (1982) Multiple Quantum Filters for Elucidating NMR Coupling Networks, *J. Am. Chem. Soc. 104*, 6800−6801.
20. Braunschweiler, L., and Ernst, R. R. (1983) Coherence Transfer by Isotropic Mixing: Application to Proton Correlation Spectroscopy, *J. Magn. Reson. 53*, 521−528.
21. Kumar, A., Ernst, R. R., and Wüthrich, K. (1980) A two-dimensional nuclear Overhauser enhancement (2D NOE) experiment for the elucidation of complete proton−proton cross-relaxation networks in biological macromolecules, *Biochem. Biophys. Res. Commun. 95*, 1−6.
22. Macura, S., and Ernst, R. R. (1980) Elucidation of Cross Relaxation in Liquids by Two-Dimensional Nmr-Spectroscopy, *Mol. Phys. 41*, 95−117.
23. Bax, A., and Davis, D. G. (1985) Practical Aspects of Two-Dimensional Transverse NOE Spectroscopy, *J. Magn. Reson. 63*, 207−213.
24. States, D. J., Haberkorn, R. A., and Ruben, D. J. (1982) A Two-Dimensional Nuclear Overhauser Experiment with Pure Absorption Phase in 4 Quadrants, *J. Magn. Reson. 48*, 286−292.
25. Piotto, M., Saudek, V., and Sklenar, V. (1992) Gradient-tailored excitation for single-quantum NMR spectroscopy of aqueous solutions, *J. Biomol. NMR 2*, 661−665.

26. Delaglio, F., Grzesiek, S., Vuister, G. W., Zhu, G., Pfeifer, J., and Bax, A. (1995) NMRPipe: A multidimensional spectral processing system based on UNIX pipes, *J. Biomol. NMR 6*, 277−293.
27. Güntert, P., Mumenthaler, C., and Wüthrich, K. (1997) Torsion angle dynamics for NMR structure calculation with the new program DYANA, *J. Mol. Biol. 273*, 283−298.
28. Pristovsek, P., Ruterjans, H., and Jerala, R. (2002) Semiautomatic sequence-specific assignment of proteins based on the tertiary structure−the program st2nmr, *J. Comput. Chem. 23*, 335−340.
29. Dauber-Osguthorpe, P., Roberts, V. A., Osguthorpe, D. J., Wolff, J., Genest, M., and Hagler, A. T. (1988) Structure and energetics of ligand binding to proteins: *Escherichia coli* dihydrofolate reductase-trimethoprim, a drug-receptor system, *Proteins 4*, 31−47.
30. *INSIGHT II User Guide* (1995) Biosym Technologies, San Diego.
31. Laskowski, R. A., Rullmannn, J. A., MacArthur, M. W., Kaptein, R., and Thornton, J. M. (1996) AQUA and PROCHECK-NMR: Programs for checking the quality of protein structures solved by NMR, *J. Biomol. NMR 8*, 477−486.
32. Brunger, A. T., Adams, P. D., Clore, G. M., DeLano, W. L., Gros, P., Grosse-Kunstleve, R. W., Jiang, J. S., Kuszewski, J., Nilges, M., Pannu, N. S., Read, R. J., Rice, L. M., Simonson, T., and Warren, G. L. (1998) Crystallography & NMR system: A new software suite for macromolecular structure determination, *Acta Crystallogr. D54* (Part 5), 905−921.
33. Chen, Y., Mant, C. T., Farmer, S. W., Hancock, R. E., Vasil, M. L., and Hodges, R. S. (2005) Rational design of α-helical antimicrobial peptides with enhanced activities and specificity/therapeutic index, *J. Biol. Chem. 280*, 12316−12329.
34. van't Hof, W., Veerman, E. C. I., Helmerhorst, E. J., and Amerongen, A. V. N. (2001) Antimicrobial peptides: Properties and applicability, *Biol. Chem. 382*, 597−619.
35. Koradi, R., Billeter, M., and Wüthrich, K. (1996) MOLMOL: A program for display and analysis of macromolecular structures, *J. Mol. Graphics 14*, 31−32.
36. Sforça, M. L., Machado, A., Figueredo, R. C., Oyama, J. S., Silva, F. D., Miranda, A., Daffre, S., Miranda, M. T., Spisni, A., and Pertinhez, T. A. (2005) The Micelle-Bound Structure of an Antimicrobial Peptide Derived from the α-Chain of Bovine Hemoglobin Isolated from the Tick *Boophilus microplus*, *Biochemistry 44*, 6440−6451.
37. Pukala, T. L., Brinkworth, C. S., Carver, J. A., and Bowie, J. H. (2004) Investigating the importance of the flexible hinge in caerin 1.1: Solution structures and activity of two synthetically modified caerin peptides, *Biochemistry 43*, 937−944.
38. Kobayashi, S., Chikushi, A., Tougu, S., Imura, Y., Nishida, M., Yano, Y., and Matsuzaki, K. (2004) Membrane translocation mechanism of the antimicrobial peptide buforin 2, *Biochemistry 43*, 15610−15616.
39. Uhrig, M. L., Couto, A. S., Alves, M. J., Colli, W., and de Lederkremer, R. M. (1997) *Trypanosoma cruzi*: Nitrogenous-base-containing phosphatides in trypomastigote forms−isolation and chemical analysis, *Exp. Parasitol. 87*, 8−19.
40. Cronan, J. E. (2003) Bacterial membrane lipids: Where do we stand? *Annu. Rev. Microbiol. 57*, 203−224.
41. Chioccola, V. L. P., Acosta-Serrano, A., Almeida, I. C., Ferguson, M. A. J., Souto-Padron, T., Rodrigues, M. M., Travassos, L. R., and Schenkman, S. (2000) Mucin-like molecules form a negatively charged coat that protects *Trypanosoma cruzi* trypomastigotes from killing by human anti-α-galactosyl antibodies, *J. Cell Sci. 113*, 1299−1307.
42. Papo, N., and Shai, Y. (2003) Can we predict biological activity of antimicrobial peptides from their interactions with model phospholipid membranes? *Peptides 24*, 1693−1703.
43. Hancock, R. E. (2001) Cationic peptides: Effectors in innate immunity and novel antimicrobials, *Lancet Infect. Dis. 1*, 156−164.
44. Vizioli, J., and Salzet, M. (2002) Antimicrobial peptides versus parasitic infections? *Trends Parasitol. 18*, 475−476.
45. Azambuja, P., Mello, C. B., D'Escoffier, L. N., and Garcia, E. S. (1989) In vitro cytotoxicity of *Rhodnius prolixus* hemolytic factor and mellitin towards different trypanosomatids, *Braz. J. Med. Biol. Res. 22*, 597−599.
46. Huang, C. M., Chen, H. C., and Zierdt, C. H. (1990) Magainin analogs effective against pathogenic protozoa, *Antimicrob. Agents Chemother. 34*, 1824−1826.
47. Barr, S. C., Rose, D., and Jaynes, J. M. (1995) Activity of lytic peptides against intracellular *Trypanosoma cruzi* amastigotes in vitro and parasitemias in mice, *J. Parasitol. 81*, 974−978.
48. Brand, G. D., Leite, J. R., Silva, L. P., Albuquerque, S., Prates, M. V., Azevedo, R. B., Carregaro, V., Silva, J. S., Sa, V. C., Brandao, R. A., and Bloch, C., Jr. (2002) Dermaseptins from *Phyllomedusa oreades* and *Phyllomedusa distincta*. Anti-*Trypanosoma cruzi* activity without cytotoxicity to mammalian cells, *J. Biol. Chem. 277*, 49332−49340.
49. Leite, J. R., Silva, L. P., Rodrigues, M. I., Prates, M. V., Brand, G. D., Lacava, B. M., Azevedo, R. B., Bocca, A. L., Albuquerque, S., and Bloch, J. (2005) Phylloseptins: A novel class of anti-bacterial and anti-protozoan peptides from the *Phyllomedusa* genus, *Peptides 26*, 565−573.
50. Jacobs, T., Bruhn, H., Gaworski, I., Fleischer, B., and Leippe, M. (2003) NK-lysin and its shortened analog NK-2 exhibit potent activities against *Trypanosoma cruzi*, *Antimicrob. Agents Chemother. 47*, 607−613.
51. Fauchere, J. L., Charton, M., Kier, L. B., Verloop, A., and Pliska, V. (1988) Amino acid side chain parameters for correlation studies in biology and pharmacology, *Int. J. Pept. Protein Res. 32*, 269−278.
52. Kyte, J., and Doolittle, R. F. (1982) A simple method for displaying the hydropathic character of a protein, *J. Mol. Biol. 157*, 105−132.
53. Eisenberg, D., Weiss, R. M., and Terwilliger, T. C. (1984) The hydrophobic moment detects periodicity in protein hydrophobicity, *Proc. Natl. Acad. Sci. U.S.A. 81*, 140−144.

BI0514515